CONDENSED
MATTER
PHYSICS

Integer quantum Hall effect and topological phase transitions in silicene

Y.L. Liu[1], G.X. Luo[2], N. Xu[2]*, H.Y. Tian[3], C.D. Ren[4]†

[1] Faculty of Electric Information Engineering, Huaiyin Institute of Technology, Huaian 223001, China

[2] Department of Physics, Yancheng Institute of Technology, Jiangsu 224051, China

[3] School of Physics and Electronic Engineering, Linyi University, Linyi 276005, China

[4] Department of Physics, Zunyi Normal College, Guizhou 563002, China

We numerically investigate the effects of disorder on the quantum Hall effect (QHE) and the quantum phase transitions in silicene based on a lattice model. It is shown that for a clean sample, silicene exhibits an unconventional QHE near the band center, with plateaus developing at $\nu = 0, \pm 2, \pm 6, \ldots$, and a conventional QHE near the band edges. In the presence of disorder, the Hall plateaus can be destroyed through the float-up of extended levels toward the band center, in which higher plateaus disappear first. However, the center $\nu = 0$ Hall plateau is more sensitive to disorder and disappears at a relatively weak disorder strength. Moreover, the combination of an electric field and the intrinsic spin-orbit interaction (SOI) can lead to quantum phase transitions from a topological insulator to a band insulator at the charge neutrality point (CNP), accompanied by additional quantum Hall conductivity plateaus.

Key words: *quantum Hall effect, silicene, quantum phase transitions*

PACS: *73.43.-f, 73.43.Nq, 72.80.Ey*

1. Introduction

Silicene is a monolayer of silicon atoms bonded together on a two-dimensional (2D) honeycomb lattice. Both silicene sheets and ribbons have been experimentally synthesized through synthesis on metal surfaces [1–4]. Silicene shares almost every remarkable property of graphene; for instance, it exhibits Dirac-like electron dispersion at the corners of the Brillouin zone. Unlike graphene, it has a buckled structure due to the large ionic radius of silicon atoms [5–7], which causes different sublattices to sit in different vertical planes with a separation of $d \approx 0.46$ Å [5, 8], as shown in figure 1. When an electric field E_z is applied perpendicular to the silicene plane, an on-site potential difference ($\Delta_z = E_z d$) will be created between different sublattices [5, 9, 10]. Moreover, a buckled structure leads to a relatively large spin-orbit gap of $\Delta_{so} \approx 1.55 - 7.9$ meV [5–8], as obtained through first-principles calculations and tight-binding calculations [7], which provides a mass to the Dirac fermions. When the strength of Δ_z becomes greater than Δ_{so}, silicene will undergo a transition from a topological insulator (TI) to a band insulator (BI) [5, 10, 11].

Under a perpendicular magnetic field B, graphene exhibits a $\sqrt{B}$-dependent Landau level (LL) spectrum and gives rise to an unusual integer quantum Hall effect (QHE). Similar to graphene, the $n \neq 0$ LLs of silicene scale as $\sqrt{B}$, whereas the $n = 0$ LL is not pinned at zero energy as in graphene [11, 12]. Therefore, silicene is expected to exhibit an exotic QHE, and the $n = 0$ LL should possess peculiar properties under the combination of a perpendicular electric field and the spin-orbit interaction (SOI). Recently, the QHE and quantum phase transitions of silicene have been investigated by many authors

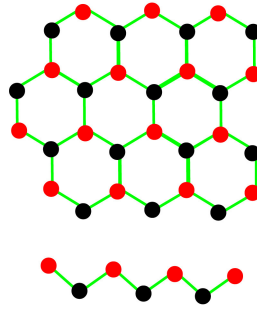*xuning79530@126.com
†renchongdan@hotmail.com

Figure 1. (Color online) Illustration of buckled silicene. The upper and lower images correspond to top and side views, respectively, of the lattice geometry. Due to the large ionic size of silicon atoms, the silicene lattice is buckled, and the two sublattices sit in vertically separated, parallel planes.

[13–17]; however, studies of the effect of disorder on the QHE in silicene, which is an essential ingredient for understanding the underlying physics of the QHE phenomenon compared with that in graphene [18], are still lacking. Therefore, it is highly desirable to numerically investigate the effect of disorder on the QHE in silicene while considering the full band structure to reveal the underlying physics of the QHE phenomenon.

In this work, we conduct a numerical study of the QHE in silicene in the presence of disorder and an electric field based on a tight-binding model. It is shown that unconventional QHE plateaus at $\nu = 0, \pm 2, \pm 6, \ldots$ are produced near the band center and conventional QHE plateaus appear near the band edges. We further map out the phase diagram for the QHE and demonstrate that the Hall plateaus disappear at strong disorder through the float-up of extended levels toward the band center. However, the $\nu = 0$ plateau is not as stable as other plateaus with the same plateau width near the band center and will disappear at a weak disorder. Under a perpendicular electric field, the spin and valley degeneracies are lifted, and the system changes from the TI phase to BI phase when the strength of the electric field exceeds the strength of the SOI.

2. Model and formalism

We consider a buckled silicene structure on a honeycomb lattice, where the A and B sublattices sit in different vertical planes, as shown in figure 1. The entire system contains L_y zigzag chains with L_x atoms in each chain, and the size of the sample could be expressed as $N = L_x \times L_y$. Under a perpendicular electric field E_z, a staggered potential $\Delta_z = E_z d$ is generated between different sublattices. In the presence of both a magnetic field and an electric field applied perpendicular to the silicene plane, the lattice model can be written in the tight-binding form as follows [7]:

$$H = \sum_{i\alpha}(\epsilon_{i\alpha} + w_{i\alpha})a_{i\alpha}^\dagger a_{i\alpha} - t \sum_{\langle i,j\rangle\alpha} \mathrm{e}^{\mathrm{i}\phi_{ij}} a_{i\alpha}^\dagger a_{j\alpha} + \mathrm{i}\frac{\lambda_{\mathrm{so}}}{3\sqrt{3}} \sum_{\langle\langle i,j\rangle\rangle\alpha\beta} \nu_{ij} a_{i\alpha}^\dagger \sigma_{\alpha\beta}^z a_{j\beta} + \Delta_z \sum_{i\alpha} a_{i\alpha}^\dagger \tau_z a_{i\alpha} , \quad (2.1)$$

where $a_{i\alpha}^\dagger$ and $a_{i\alpha}$ are the creation and annihilation operators at the i-th discrete site with spin polarization α and the $\langle i,j\rangle$ ($\langle\langle i,j\rangle\rangle$) run over all nearest-neighbor (next-nearest-neighbor) hopping sites. The first term represents the on-site energy and random disorder, where the on-site disorder energy w_i is uniformly distributed in the range $w_i \in [-W/2, W/2]t$ in terms of the disorder strength W. The second and third terms represent the nearest and next-nearest couplings with the effective SOI λ_{so}, where $\sigma = (\sigma_x, \sigma_y, \sigma_z)$ is the Pauli spin matrices and $\nu_{ij} = +1$ and $\nu_{ij} = -1$ correspond to anticlockwise and clockwise next-nearest-neighboring hopping, respectively, with respect to the positive z axis. The final term represents the lattice potential resulting from different sublattices in the perpendicular electric field E_z, where τ_z is the Pauli matrix of the sublattice. In the presence of a magnetic field B, a Peierls phase factor ϕ_{ij} is added to the hopping interactions, where $\phi_{ij} = \int_i^j \vec{A} \cdot \mathrm{d}\vec{l}/\phi_0$, with the vector potential $\vec{A} = (-By, 0, 0)$ and

$\phi_0 = \hbar/e$. The magnetic flux per hexagon is $\phi = 2\pi/M$, where M is an integer. The total flux through the sample, $N\phi/4\pi$, is taken to be an integer. When M is equal to L_x or L_y, the magnetic periodic boundary conditions are reduced to ordinary periodic boundary conditions. Here, we disregard the Rashba SOI because it is weak in comparison with the intrinsic SOI [7].

In the presence of an electric field, the spin degeneracy is broken; therefore, it is convenient to investigate the Hall conductivity separately for each spin. We use the symbol s ($s = \uparrow, \downarrow$) to define the spin up or spin down. The eigenstates $|\alpha^s\rangle$ and eigenenergies ϵ_α^s for each spin are obtained through exact diagonalization of the Hamiltonian in equation (2.1), and the Hall conductivity for different spins σ_{xy}^s is calculated using the Kubo formula [18]:

$$\sigma_{xy}^s = \frac{ie^2\hbar}{S} \sum_{\alpha,\beta} \frac{\langle \alpha^s|V_x^s|\beta^s\rangle \langle \beta^s|V_y^s|\alpha^s\rangle - \text{h.c.}}{(\epsilon_\alpha^s - \epsilon_\beta^s)^2}, \tag{2.2}$$

where S is the area of the sample and V_x^s and V_y^s are the velocity operators of spin s. The total Hall conductivity of the system is $\sigma_{xy} = \sigma_{xy}^\uparrow + \sigma_{xy}^\downarrow$. It is hoped that our results will suggest new potential directions for the experimental realization of the QHE and topological insulators.

3. Results and discussion

In what follows, we will discuss the Hall conductivity σ_{xy} and the quantum phase transitions in silicene. In our calculations, the hopping integrals and the SOI strength are taken to be $t = 1.6$ eV and $\lambda_{so} = 0.04t$, respectively; the temperature is set to $T = 0$ K, and the disorder is averaged over 800 sample configurations.

We first focus on the Hall conductivity and the electron density of states as functions of the electron Fermi energy E_f for a clean sample ($W = 0$) under zero electric field; the results are shown in figure 2. The system size is taken to be $N = 288 \times 32$ and the magnetic flux is taken to be $\phi = 2\pi/96$ (corresponding to approximately 822 T [19]) to illustrate the overall picture of the QHE throughout the entire energy band.
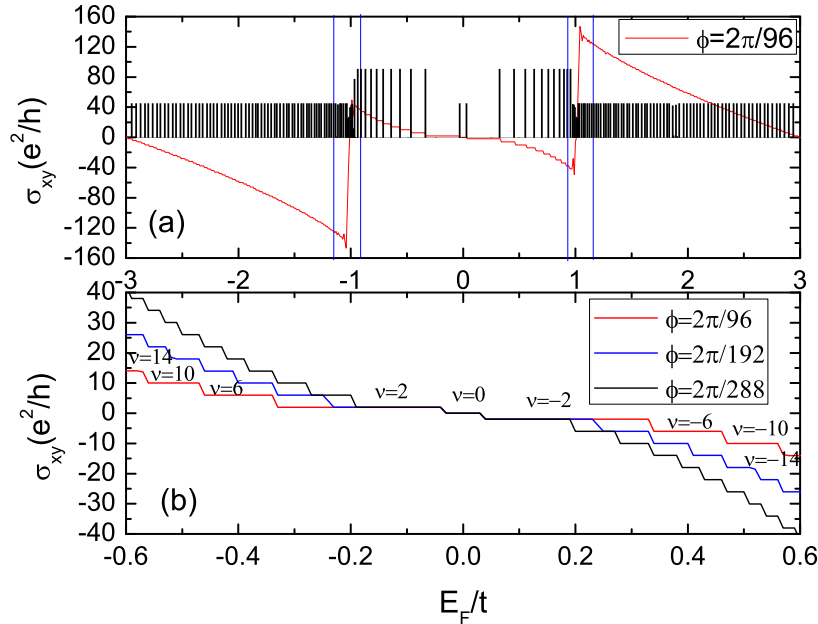

Figure 2. (Color online) (a) The Hall conductivity σ_{xy} and electron density of states (in units of 1) throughout the entire energy band with a magnetic flux of $\phi = 2\pi/96$. (b) The Hall conductivity near the band center for different magnetic fluxes. The disorder strength is $W = 0$, and the electric field strength is $\Delta_z = 0$; the system size is $N = 288 \times 32$.

It is shown in figure 2 (a) that discrete LLs appear in the system and constitute a nonzero density of states. The LLs near the band center are four-fold degenerate due to the two spin components and two Dirac points, except for the two center $n = 0$ LLs adjacent to the gap, which show a spin splitting: the upper one is the $n = 0$ spin-up LL, and the lower one is the $n = 0$ spin-down LL. The LL above (below) the spin-up (spin-down) $n = 0$ LL is the $n = 1$ ($n = -1$) LL, and so on. Therefore, at the band center, the quantum Hall conductivity $\sigma_{xy} = \nu e^2/h$ is quantized according to the unconventional quantization rule $\nu = g_s(k - 1/2)e^2/h$ ($k = 1, 2, \ldots$) beyond the gap, where $g_s = 4$ is the LL degeneracy. However, a zero Hall plateau appears in the energy gap ($-\lambda_{so} \leqslant E_f \leqslant \lambda_{so}$) because the two $n = 0$ LLs reside at $E_f = \pm\lambda_{so}$ and each contributes a Hall conductivity of $\pm e^2/h$, respectively, to σ_{xy}. A similar zero quantum Hall plateau induced by the quantum spin Hall (QSH) gap can also appear in graphene under a strong magnetic field; however, it is induced by Zeeman splitting rather than by the SOI [20]. In figure 2 (b), the quantization rule for the Hall conductance in this unconventional region is shown for three different ϕ. It is shown that more quantum plateaus appear with a decreasing ϕ, but the $\nu = 0$ plateau is not affected by a change in the magnetic field.

As each additional LL is occupied, the total Hall conductivity increases by $g_s e^2/h$ as a result of the spin and valley degeneracy. When the energy reaches $E_f = \pm t$, which are the van Hove singularities, the Hall plateaus become indiscernible and the system changes to exhibit the conventional QHE as it exceeds the critical region, as indicated by the two blue lines. Similar to those in graphene [18, 21], these crossover regions correspond to a transport regime, in which the Hall resistance changes sign and the longitudinal conductivity exhibits a metallic behavior. At the band edges, the LLs are two-fold degenerate due to the two spin components, and a conventional QHE emerges, with the Hall conductivity quantized as $\sigma_{xy} = kg_s e^2/h$ ($k = 1, 2, \ldots$), where $g_s = 2$ because there is a spin degeneracy only.

Now, we investigate the effect of random disorder on the QHE in silicene. In figure 3, the Hall conductance near the band center is shown for different disorder strengths, with a magnetic flux of $\phi = 2\pi/96$ and a system size of $N = 288 \times 32$. It is shown that the higher plateaus (with larger $|\nu|$) become less distinct and eventually disappear with an increasing W. At $W = 0.05$, the plateaus at $\nu = 0, \pm2, \pm6, \pm10, \pm14$ remain well quantized, whereas all plateaus except the $\nu = \pm2$ plateau disappear at $W = 2.0$. By contrast, as shown in the lower inset of the panel, for the QHE near the band edge, all
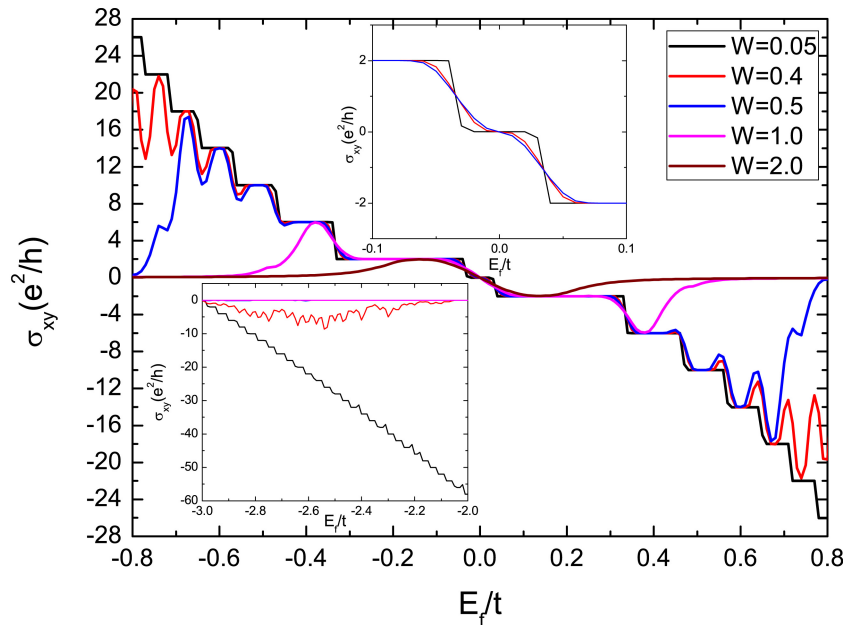

Figure 3. (Color online) Calculated Hall conductivity σ_{xy} as a function of the electron Fermi energy for different disorder strengths. The two insets show the Hall conductivity near the lower band edge and the central Hall plateau $\nu = 0$. The magnetic flux and system size are $\phi = 2\pi/96$ and $N = 288 \times 32$, respectively.

plateaus are destroyed at a low disorder strength of $W = 0.5$. The center plateau ($\nu = 0$) remains distinct at a small disorder strength of $W = 0.05$; however, it narrows at $W = 0.4$ and nearly disappears at a disorder strength of $W = 0.5$ (the higher insert in figure 3). Obviously, the $\nu = 0$ plateau is not as robust as the one at $\nu = 14$, which has approximately the same initial width as the $\nu = 0$ plateau but still has a narrow, yet finite width at $W = 0.5$. This is because the magnetic field breaks the time-reversal symmetry of the QSH states in the energy gap, and the $\nu = 0$ states become unstable under a weak disorder.

Finally, we numerically investigate the quantum phase transition from a two-dimensional TI to a trivial insulator under an external perpendicular electric field with an on-site potential difference of Δ_z; the results are shown in figure 4. When $\Delta_z = 0$, the $n = 0$ LLs are valley degenerate and spin split — the spin-up LL is located at $E_f = \lambda_{so}$, and the spin-down LL is located at $E_f = -\lambda_{so}$. They have the same density of states and make Hall conductivity contributions of $\pm e^2/h$, leading to zero Hall conductivity near the Dirac point. In the presence of an electric field, the valley degeneracy is resolved, which results in four $n = 0$ states; two are from the K valley, and two are from the K' valley. For a pair of spins from different valleys, there is a gap between them that can be tuned by adjusting the electric field. However, the gap between the two spins in each valley (K or K') is fixed at the SOI strength, λ_{so}. As Δ_z increases, the valley split is enhanced; thus, the spin-up state from the K valley descends and the spin-down state from the K' valley ascends. When $\Delta_z < \Delta_{so}$, the two states are still above and below the Dirac point; therefore, the total system is still a TI, and Hall plateaus appear at $\nu = 0, \pm 1, \pm 2$ near the Dirac point, as shown in figure 4 (b). At the critical point $\Delta_z = \Delta_{so}$, the two states coincide at $E_f = 0$ and the system transits into a semi-metallic state, with Hall plateaus appearing at $\nu = 0, \pm 2$ near the Dirac point, as shown in figure 4 (c). When $\Delta_z > \Delta_{so}$, band inversion occurs, with the spin-down state from the K' valley shifting from negative to positive and the spin-up state from the K valley shifting from positive to negative; the system enters the BI regime, and Hall plateaus develop at $\nu = 0, \pm 1, \pm 2$. In figure 4 (b) and (d), the $\nu = \pm 1$ plateaus that are contributed by one spin state from one valley arise only from the breaking of the valley degeneracy. In fact, $\nu = \pm 1$ Hall plateaus can also appear in graphene, in which case they originate from the long-range Coulomb interaction [22] or the breaking of the spin and valley degeneracies [20].
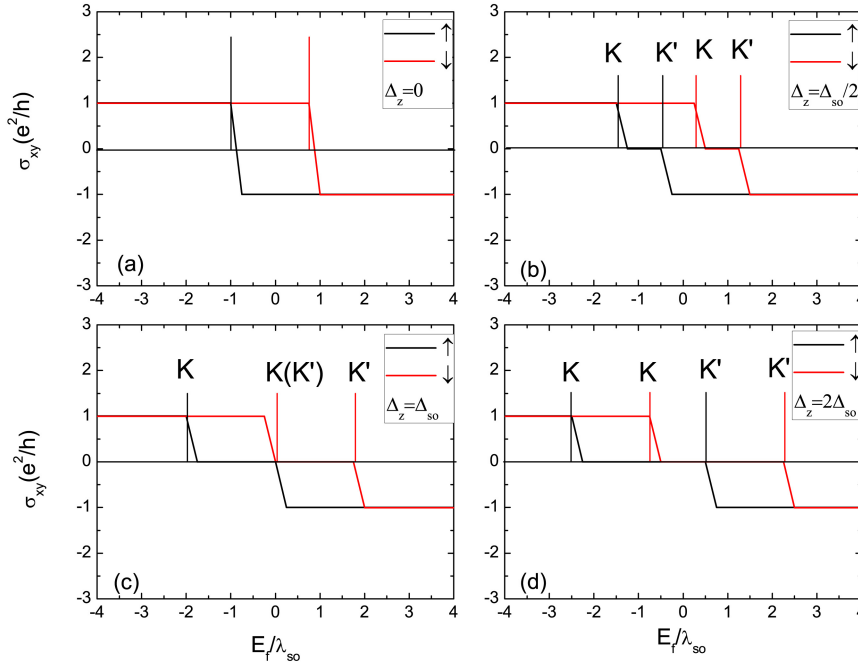

Figure 4. (Color online) Spin-dependent Hall conductivity and electron density of states of the $n = 0$ states for different on-site potential differences Δ_z. The black and red lines correspond to the spin-down and spin-up states, respectively. The notation K (K') in the figure indicates the state from the K (K') valley. The magnetic flux and system size are $\phi = 2\pi/96$ and $N = 288 \times 32$, respectively.

4. Conclusion

In conclusion, we have numerically investigated the effects of disorder on the QHE and the quantum phase transitions in silicene under a perpendicular electric field. It is shown that Hall plateaus develop at $v = 0, \pm2, \pm6, \ldots$ near the band center, whereas conventional quantum Hall plateaus appear near the band edges. The phase diagram indicates that the Hall plateaus gradually disappear toward the band center with an increasing disorder strength, which causes higher plateaus to disappear first. However, the $v = 0$ plateau is not robust and disappears at a relatively weak disorder strength. In the presence of an electric field, the valley degeneracy of the two $n = 0$ LLs is broken, which results in a quantum phase transition at the CNP together with the unconventional plateaus in the QHE. The derived results also apply to isostructural germanene, whose SOI strength is even higher ($\Delta_{so} = 43$ meV with $d = 0.66$ Å). Due to the strong SOI and electric field, the QHE in silicene and germanene will be unaffected by temperature. Therefore, the QHE and quantum phase transitions in silicene and germanene can be experimentally observed and tuned at a finite temperature. Electrical controllability in silicene and germanene is of great significance for the development of electrically tunable spintronic and valleytronic devices.

Acknowledgements

References

1. Majzik Z., Tchalala M.R., Švec M., Hapala P., Enriquez H., Kara A., Mayne A.J., Dujardin G., Jelínek P., Oughaddou H., J. Phys.: Condens. Matter, 2013, **25**, No. 22, 225301, doi:10.1088/0953-8984/25/22/225301.
2. De Padova P., Quaresima C., Ottaviani C., Sheverdyaeva P.M., Moras P., Carbone C., Topwal D., Olivieri B., Kara A., Oughaddou H., Aufray B., Le Lay G., Appl. Phys. Lett., 2010, **96**, No. 26, 261905, doi:10.1063/1.3459143.
3. Vogt P., de Padova P., Quaresima C., Avila J., Frantzeskakis E., Asensio M.C., Resta A., Ealet B., Le Lay G., Phys. Rev. Lett., 2012, **108**, No. 15, 155501, doi:10.1103/PhysRevLett.108.155501.
4. Chiappe D., Scalise E., Cinquanta E., Grazianetti C., van den Broek B., Fanciulli M., Houssa M., Molle A., Adv. Mater., 2014, **26**, No. 13, 2096, doi:10.1002/adma.201304783.
5. Drummond N.D., Zólyomi V., Fal'ko V.I., Phys. Rev. B, 2012, **85**, No. 7, 075423, doi:10.1103/PhysRevB.85.075423.
6. Liu C.-C., Feng W., Yao Y., Phys. Rev. Lett., 2011, **107**, No. 7, 076802, doi:10.1103/PhysRevLett.107.076802.
7. Liu C.-C., Jiang H., Yao Y., Phys. Rev. B, 2011, **84**, No. 19, 195430, doi:10.1103/PhysRevB.84.195430.
8. An X.-T., Zhang Y.-Y., Liu J.-J., Li S.-S., J. Phys.: Condens. Matter, 2012, **24**, No. 50, 505602, doi:10.1088/0953-8984/24/50/505602.
9. Ni Z., Liu Q., Tang K., Zheng J., Zhou J., Qin R., Gao Z., Yu D., Lu J., Nano Lett., 2012, **12**, No. 1, 113, doi:10.1021/nl203065e.
10. Ezawa M., New J. Phys., 2012, **14**, No. 3, 033003, doi:10.1088/1367-2630/14/3/033003.
11. Tabert C.J., Nicol E.J., Phys. Rev. B, 2013, **88**, No. 8, 085434, doi:10.1103/PhysRevB.88.085434.
12. Ullah A., Sabeeh K., J. Phys.: Condens. Matter, 2014, **26**, No. 50, 505303, doi:10.1088/0953-8984/26/50/505303.
13. Ezawa M., J. Phys. Soc. Jpn., 2012, **81**, No. 6, 064705, doi:10.1143/JPSJ.81.064705.
14. Tahir M., Schwingenschlögl U., Sci. Rep., 2013, **3**, 1075, doi:10.1038/srep01075.
15. Shakouri Kh., Vasilopoulos P., Vargiamidis V., Hai G.-Q., Peeters F.M., Appl. Phys. Lett., 2014, **104**, No. 21, 213109, doi:10.1063/1.4878509.
16. Shakouri Kh., Vasilopoulos P., Vargiamidis V., Peeters F.M., Phys. Rev. B, 2014, **90**, No. 23, 235423, doi:10.1103/PhysRevB.90.235423.
17. Shakouri Kh., Vasilopoulos P., Vargiamidis V., Peeters F.M., Phys. Rev. B, 2014, **90**, No. 12, 125444, doi:10.1103/PhysRevB.90.125444.
18. Sheng D.N., Sheng L., Weng Z.Y., Phys. Rev. B, 2006, **73**, No. 23, 233406, doi:10.1103/PhysRevB.73.233406.
19. Cresti A., Grosso G., Parravicini G.P., Phys. Rev. B, 2008, **77**, No. 11, 115408, doi:10.1103/PhysRevB.77.115408.

20. Young A.F., Sanchez-Yamagishi J.D., Hunt B., Choi S.H., Watanabe K., Taniguchi T., Ashoori R.C., Jarillo-Herrero P., Nature, 2014, **505**, No. 7484, 528, doi:10.1038/nature12800.
21. Hatsugai Y., Fukui T., Aoki H., Phys. Rev. B, 2006, **74**, No. 20, 205414, doi:10.1103/PhysRevB.74.205414.
22. Sheng L., Sheng D.N., Haldane F.D.M., Balents L., Phys. Rev. Lett., 2007, **99**, No. 19, 196802, doi:10.1103/PhysRevLett.99.196802.

Цілочисловий квантовий Голів ефект та топологічні фазові переходи у сіліцені

Я.Л. Ліу[1], Г.Х. Луо[2], Н. Сюй[2], Ґ.Я. Тіань[3], Ц.Д. Рен[4]

[1] Факультет електричної інформаційної техніки, Технологічний інститут Хуаинь, Хуайань 223001, Китай

[2] Відділ фізики, Технологічний інститут Яньчен, Цзянсу 224051, Китай

[3] Інститут фізики та електронної інженерії, Університет Ліньї, Ліньї 276005, Китай

[4] Відділ фізики, Нормальний коледж Цзуньї, Ґуйчжоу 563002, Китай

Проведено числове дослідження впливу безладу на квантовий Голів ефект (КГЕ) та квантові фазові переходи у сіліцені на основі ґраткової моделі. Показано, що у випадку чистого зразка, сіліцен проявляє нетрадиційний КГЕ поблизу центру зони, де утворюються плато при $\nu = 0, \pm 2, \pm 6, \ldots$, і традиційний КГЕ поблизу країв зони. При наявності безладу, плато Гола можуть бути зруйновані за рахунок спливання розтягнутих рівнів в напрямку до центру зони, де першими зникають вищі плато. Однак, центр $\nu = 0$ плато Гола є більш чутливим до безладу і зникає при відносно слабій силі безладу. Крім того, поєднання електричного поля та властивої спін-орбітальної взаємодії може призвести до квантових фазових переходів від топологічного діелектрика до зонного діелектрика у точці нейтральності заряду, що супроводжується утворенням додаткових плато квантової провідності Гола.

Ключові слова: квантовий Голів ефект, сіліцен, квантові фазові переходи